

Transition temperature and magnetic properties of the granular Ising model in two dimensions studied by Monte Carlo simulations: Impact of intragrain spin structure

M. D. Leblanc, M. L. Plumer, J. P. Whitehead, and J. I. Mercer

Department of Physics and Physical Oceanography, Memorial University of Newfoundland, St. John's, Newfoundland, Canada A1B 3X7
(Received 19 May 2010; revised manuscript received 31 August 2010; published 23 November 2010)

Monte Carlo simulations are performed on a stacked square lattice model of weakly interacting magnetic grains composed of Ising spins. The role of intragrain spin structure on thermal properties are investigated in this simple representation of granular recording media. Various thermodynamic quantities are calculated using a cluster-flip algorithm which exhibit anomalies corresponding to both intragrain and intergrain ordering. In the single-layer case, the intergrain transition temperature vs intergrain exchange coupling strength exhibits a crossover to a nonlinear regime where the intragrain spin structure becomes increasingly important. Corresponding results on multilayer systems are shown to be in good agreement with scaling theory. Preliminary magnetization vs applied field (M - H) loops are also calculated as a function of temperature and indicate the possible effect of the grain spin structure.

DOI: [10.1103/PhysRevB.82.174435](https://doi.org/10.1103/PhysRevB.82.174435)

PACS number(s): 75.40.Mg, 75.40.Cx, 75.50.Ss, 75.70.Ak

I. INTRODUCTION

Traditional formulations of micromagnetic simulations of magnetic recording processes based on the Landau-Lifshitz-Gilbert dynamic equations have enjoyed remarkable successes over the past 20 years.^{1,2} The fundamental assumption of micromagnetics is that there are well-defined regions with a uniform magnetization of constant magnitude, \mathbf{M}_i , which interact via exchange and magnetostatic forces. In the case of current recording media based on highly anisotropic cobalt alloys, these regions are taken to be the magnetically separated grains which are typically 8–9 nm in diameter and are composed of hundreds to thousands of atomic spins. We refer to this as the rigid grain approximation (RGA). In the case of conventional recording media, the RGA may be justified by the fact that the intragrain spin-spin ferromagnetic exchange interaction is typically 10–100 times larger than intergrain exchange. In addition, temperatures relevant for typical recording processes are about one-quarter of the Curie temperature for cobalt ($T_C=1400$ K) so that thermal effects are not obviously important. Due to reductions in bit size, the need for more accurate models, and the increasingly important role of thermal effects [as in heat-assisted magnetic recording (HAMR) (Refs. 3 and 4)], there has been an exploration of modified approaches which go beyond the RGA and consider effects due to intragrain spin degrees of freedom.^{5–8} As grain sizes shrink, surface spins can play an increasingly important role in determining reversal mechanisms. This is due not only to modifications in surface-exchange interactions arising from simple geometrical arguments but also to a reduction in surface-spin anisotropy. These effects can lead to modifications in grain magnetic moments and magnetic field-induced reversal mechanisms important for the recording process.^{9–14}

In this work, we explore some limitations of the RGA within the context of a simple model that includes explicitly the internal atomic spins of a system of interacting granular magnetic moments. Monte Carlo simulations are performed on a model with grains composed of $L' \times L' \times z$ Ising spins with strong nearest-neighbor intragrain (spin-spin) exchange

interactions J' and weaker intergrain exchange J between the two-dimensional (2D) lattice consisting of $L \times L$ grains. We refer to this model as the granular Ising model. The granular Ising model may be viewed as a simple first approximation to a more realistic Heisenberg model with strong anisotropy (currently under investigation) representing recording media based on cobalt alloys. In order to address equilibration issues that arise as a consequence of the large difference in the interaction energies in this model, the simulations utilize a combination of a cluster-flip Wolff¹⁵ and Metropolis algorithms. We evaluate a number of thermodynamic quantities that reflect the degree of intragrain and intergrain ordering of the spins. From these we are able to distinguish these regimes where the RGA is valid and where it is not. We also study the hysteresis associated with the reversal of the magnetization in an applied field for $T < T_c$ and examine the impact of the intragrain spins in determining the coercivity.

The paper is structured as follows. The granular Ising model and Monte Carlo simulation techniques are described in Sec. II. In Sec. III, results for various equilibrium properties: magnetization, heat capacity, and susceptibility are presented for several values of exchange, grain dimensions and film thickness and certain key properties described within the context of simple models. In Sec. IV, M - H loops for the model are presented and we finish in Sec. V by drawing some conclusions regarding the significance of the results obtained from this series of simulations.

II. ISING MODEL OF GRANULAR RECORDING MEDIA

The model studied here consists of a system of N Ising spins on a stacked square lattice. The lattice is subdivided into L^2 grains with each grain represented by a $L' \times L' \times z$ rectangular prism. The spins are coupled through a nearest-neighbor exchange interaction. We denote by J' the exchange constant for the nearest-neighbor pairs that are located within the same grain and by J for the nearest-neighbor pairs that straddle the grain boundaries. We choose $J' = 1$ and consider values of J that lie in the range $0 \leq J \leq 1$. We assume periodic boundary conditions in lateral ($L \times L$) direc-

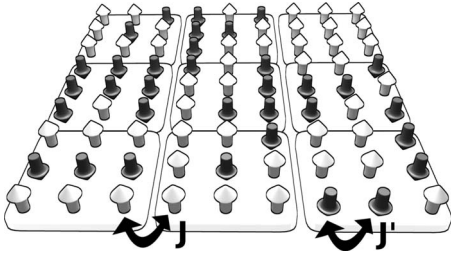


FIG. 1. Schematic of the granular Ising model showing 3×3 grains each composed of 3×3 spins with intragrain exchange J' and intergrain exchange J .

tions but not in the perpendicular (z) direction. Figure 1 shows a schematic model for a system consisting of $L^2=9$ grains, each with $(L')^2=9$ spins and $z=1$. The model Hamiltonian is given by

$$\mathcal{H} = - \sum_{\langle ij \rangle} J_{ij} S_i S_j - H \sum_i S_i, \quad (1)$$

where the first sum is over nearest-neighbor pairs, $S_i = \pm 1$, $J_{ij} = J$ or J' , and H is the applied magnetic field. We denote the number of spins in each grain by $N_g = L' \times L' \times z$ and the number of nearest-neighbor bonds between each grain as $A_g = L' \times z$. We refer to the single-layer ($z=1$), homogeneous ($J'=J$) simply as the 2D Ising model.

Labeling the individual grains by the index I , we define the average magnetization of the I th grain by

$$M_I = \frac{1}{N_g} \left| \sum_{j \in I} S_j \right|, \quad (2)$$

where $\sum_{j \in I}$ denotes the sum over all $L' \times L' \times z$ spins in grain I . The thermal average over all grain magnetizations is thus given by

$$M_g(T) = \frac{1}{L^2} \left\langle \sum_I M_I \right\rangle. \quad (3)$$

The total system magnetization is defined through

$$M(T) = \frac{1}{N} \left\langle \left| \sum_i S_i \right| \right\rangle, \quad (4)$$

where i is summed over all N lattice sites. In addition, the total magnetic susceptibility was calculated using

$$\chi(T) = \beta N (\langle M(T)^2 \rangle - \langle M(T) \rangle^2), \quad (5)$$

where $\beta = 1/T$ and the specific heat is given by

$$C(T) = \frac{\beta^2}{N} (\langle E(T)^2 \rangle - \langle E(T) \rangle^2). \quad (6)$$

To enhance equilibration, a combination of the Metropolis and a Wolff cluster-flip algorithm was used. In order for the cluster-flip algorithm to satisfy detailed balance while maintaining an acceptance ratio of unity, the standard probability for adding a spin to the cluster,¹⁵ $P_{J'} = 1 - e^{-2\beta J'}$, was used for spins inside a grain while a similar probability, $P_J = 1 - e^{-2\beta J}$, was used when determining whether to add a spin or

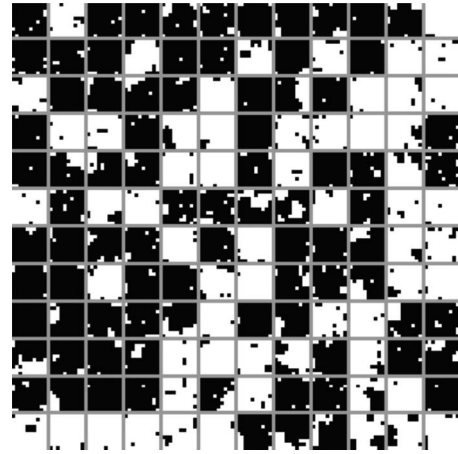


FIG. 2. Spin configuration in the single-layer ($z=1$) granular Ising model with $L=12$, $L'=10$, $J=0.03$, and $T=1.79$. Up and down spins are shown as black and white points and grain boundaries as gray lines.

not between grains. An iteration over each spin in the lattice using the Metropolis procedure and one cluster attempt with the Wolff algorithm was defined as one Monte Carlo Step (MCS). MCS₀ initial steps were discarded for equilibration. Typical runs used to obtain the results presented below had MCS₀=5000 and MCS=50 000. As an initial test of the algorithm, we verified for $N=120 \times 120 \times 1$ spins and $J=J'=1$ that the model exhibits the onset of ferromagnetic order at $T_c=2.28$ as expected for the 2D Ising model.

III. RESULTS

In this section we present the results for the intragrain and intergrain ordering from a series of simulations at $H=0$ for various values of J , L' , and z . We first consider the case $z=1$ as this reveals many of the key features of the present analysis. Results are presented for $L=12$ and $L'=5$ or 10 . A snapshot of a typical spin configuration is illustrated in Fig. 2 for the case $L'=10$, $J=0.03$, and $T=1.79$.

The spin configuration shown in Fig. 2 shows the spins to be highly ordered within the grain while the grains themselves show a considerable degree of disorder. The intragrain ordering is clearly seen in Fig. 3 which shows the grain magnetization defined by Eq. (3) as a function of temperature for several values of J and L' . The results show that the intragrain magnetization is relatively insensitive to the value of J and is at least qualitatively similar to the magnetization for a finite-size 2D Ising system. The ordering of the spins within the grains also gives rise to a well-defined peak in the heat-capacity curves shown in Fig. 4 for the specific case $L'=10$. Denoting the location of the upper peak in the heat capacity by T'_c , we note that both the location and the shape of the heat-capacity curve in the vicinity of T'_c are insensitive to the value of J . We also note that the value of $T'_c \approx 2.0$ we obtain from the heat-capacity curve is close to the value for the 2D Ising model.

The temperature dependence of the intergrain order is reflected in the magnetization curves shown in Fig. 5. In con-

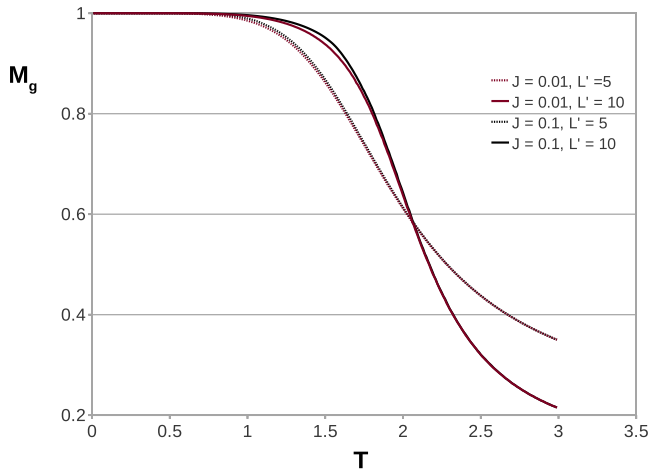


FIG. 3. (Color online) Grain magnetization vs temperature in the single-layer ($z=1$) granular Ising model with $L=12$ for two grain sizes $L'=5$ and $L'=10$ and two values of $J=0.01$ and $J=0.1$ as shown in the legend.

trast to the intragrain magnetization, the intergrain magnetization shows a strong dependence on the value of J , most notably in the temperature that marks the onset of intergrain magnetic ordering, which we denote by T_c . The onset of this intergrain magnetic ordering is also reflected in the peaks in the magnetic susceptibility presented in Fig. 6 and in the very small low-temperature peaks seen in the heat capacity in Fig. 4.

The value of intergrain ordering temperature T_c , defined by the peak in the susceptibility is plotted as a function of J in Fig. 7 for $L'=5$ and 10. In both cases we see that, for low values of J , T_c shows a linear dependence on J while for larger values of J the transition temperature deviates significantly from linear behavior. This deviation of the transition temperature from the linear dependence observed for larger values of J is more pronounced for the case $L'=10$, which, as will be shown, reflects the increasing importance of the intragrain fluctuations as the size of the grains increase.

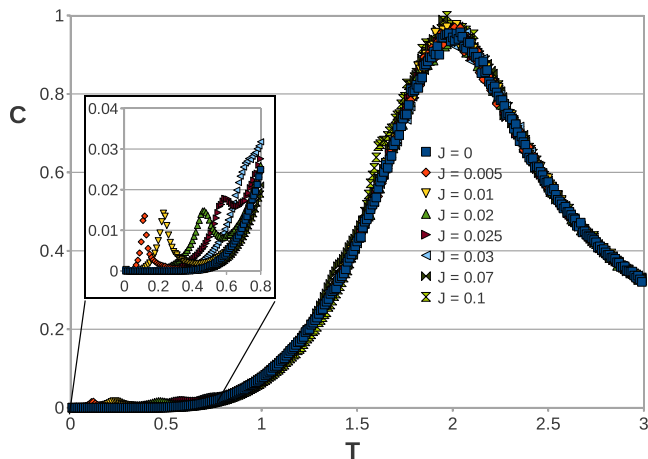


FIG. 4. (Color online) Heat capacity vs temperature in the single layer ($z=1$) granular Ising model with $L=12$ and $L'=10$ as a function of intergrain coupling J (values shown in the legend). Upper and lower peaks correspond to T'_c and T_c , respectively.

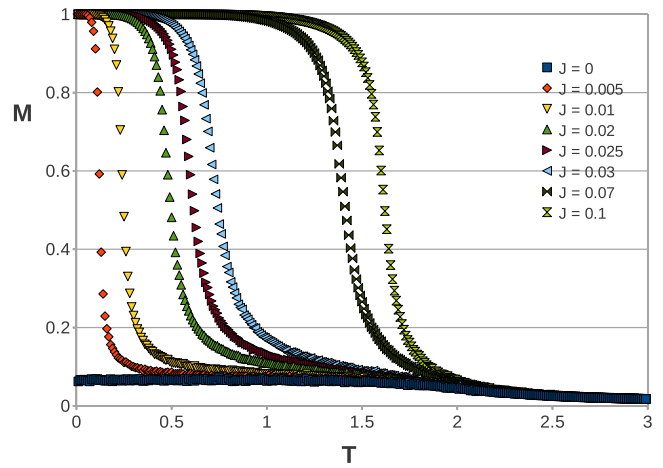


FIG. 5. (Color online) Total magnetization vs temperature in the single-layer ($z=1$) granular Ising model with $L=12$ and $L'=10$ as a function of intergrain coupling J (values shown in the legend).

Extending the analysis to the multilayer case ($z > 1$) allows for a broader understanding of the interplay between intergrain coupling, intragrain coupling, and grain size. Simulations were performed with $z=5$ and $z=10$ layers, grain sizes $L'=5$ and $L'=10$ on systems with 12×12 and 24×24 grains. Examples of results for the magnetization, susceptibility, and heat capacity that are used to estimate T'_c and T_c in the multilayer case are plotted as a function of temperature in Figs. 8–10. Within the accuracy of the simulations, the values of T'_c are insensitive to the specific value of J , depending only on the variables z and L' . The values for T'_c obtained for $J \leq 0.1$ from the simulations are summarized in Table I.

Table I includes simulation results for $J=J'=1$ which corresponds to the case of $L' \approx \infty$. Theoretical estimates of uniform layered systems can also be made based on scaling analysis.¹⁶ This yields the relation $T'_c(z) = T_0 f'(z)$, where $T_0 \approx 4.51$ denotes the transition temperature of the bulk mate-

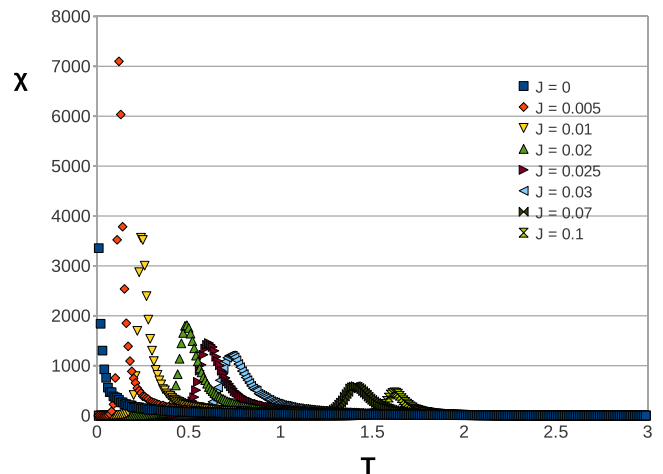


FIG. 6. (Color online) Susceptibility vs temperature in the single-layer ($z=1$) granular Ising model with $L=12$ and $L'=10$ as a function of intergrain coupling J (values shown in the legend). Peaks correspond to T_c .

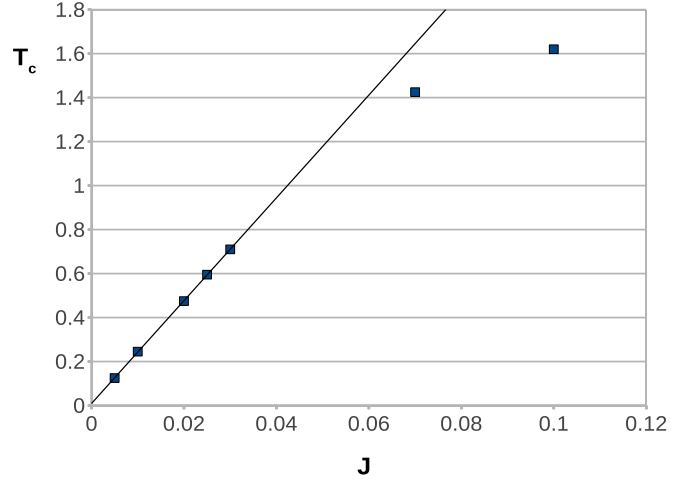
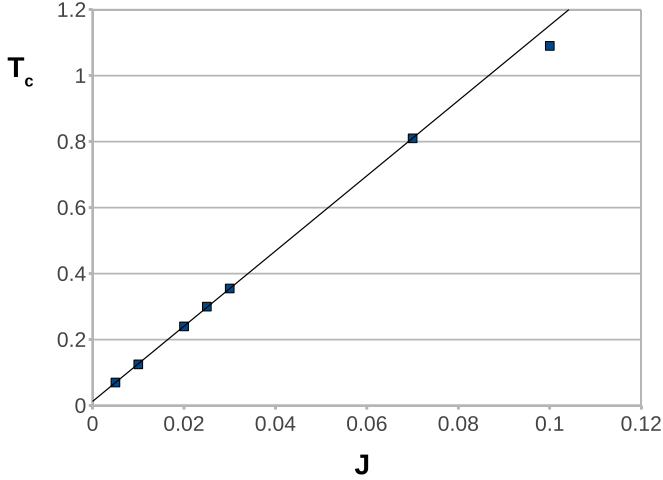


FIG. 7. (Color online) T_c vs J in the single-layer ($z=1$) granular Ising model with $L=12$ and $L'=5$ (left) or $L'=10$ (right).

rial with $J'=1.0$, $f(1) \approx 2.27/4.51 \approx 0.5$ while for $z \geq 3$ the function $f(z)$ is given by

$$f(z) = 1 - \frac{b}{z^{1/\nu}} \left(1 - \frac{a}{z} \right) \quad (7)$$

with $a=1.37572$, $b=1.92629$, and $\nu=0.6289$. Estimates based on this theory of $T'_c(z)$ are included in parenthesis in Table I (in the last column) and show good agreement with the simulations.

In order to estimate T'_c for finite L' and z we note that the correlation length for the 2D Ising model is given asymptotically by

$$\xi'(T)^{-1} = 4 \left(\frac{J'}{T} - \frac{J'}{T'_c} \right). \quad (8)$$

We estimate the grain magnetization melting temperature by the condition $\xi'[T'_c(L', z)] \approx L'$, and setting $T'_c = T'_c(z)$ we obtain the following expression for $T'_c(L', z)$:

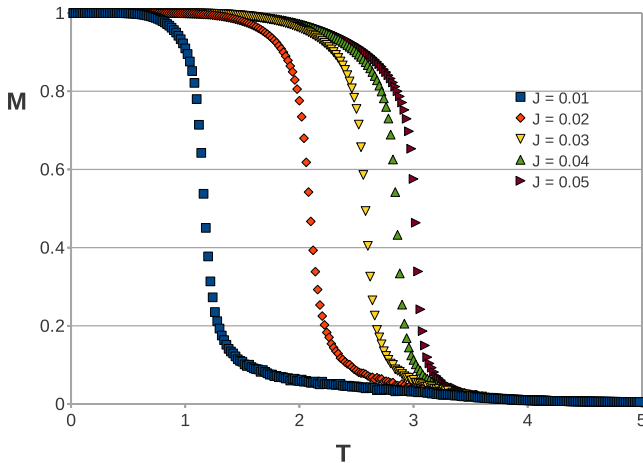


FIG. 8. (Color online) Magnetization vs temperature for different values of J shown in the legend. Here, $L'=10$ and $z=10$.

$$T'_c(L', z) \approx \frac{T'_c(z)}{1 + T'_c(z)/4J'L'}. \quad (9)$$

Estimates for $T'_c(L, z)$ calculated from Eq. (9) are also included in Table I for $L'=5, 8$, and 10 . A comparison with the results obtained from the simulations indicate that, despite the very approximate nature of Eq. (9), the results are in reasonable agreement with this analysis and certainly show the correct systematic dependence of T'_c on the dimensions of the grains.

The above analysis of the dependence of T'_c on the dimensions of the grain suggests that for $T \ll T'_c$ we have $\xi'(T) \ll L'$ and hence, to a good approximation, the magnetization within an individual grain may be considered uniform and close to saturation. It is therefore reasonable to expect the RGA to be valid for $T_c \ll T'_c$. Separating intragrain and intergrain contributions to the exchange energy, we express the Hamiltonian given by Eq. (1) as

$$\mathcal{H} = -J' \sum_I \sum_{\langle ij \rangle \in I} S_i S_j - J \sum_{\langle IJ \rangle} \left(\sum_{\langle ij \rangle \in I \cap J} S_i S_j \right) - H \sum_I \sum_{i \in I} S_i, \quad (10)$$

where $\sum_{\langle ij \rangle \in I} S_i S_j$ denotes the sum over all pairs of nearest-neighbor spins contained in the I th grain, $\sum_{\langle IJ \rangle}$ denotes the

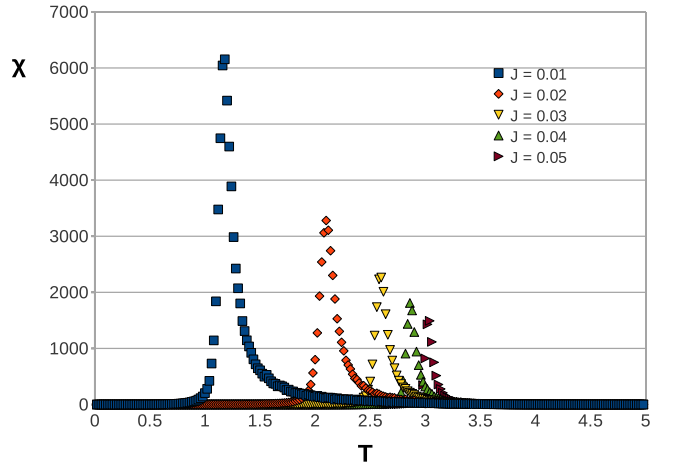


FIG. 9. (Color online) Susceptibility vs temperature for different values of J shown in the legend. Here, $L'=10$ and $z=10$.

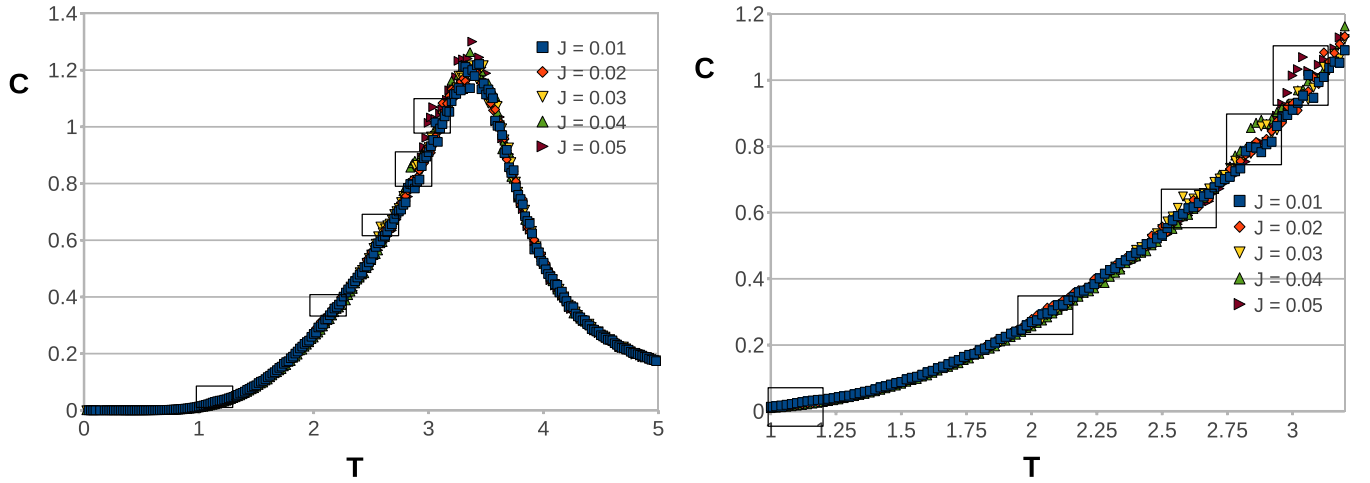


FIG. 10. (Color online) Heat capacity for different values of J shown in the legend. Here, $L'=10$ and $z=10$. Boxed region show peaks where $T \approx T_c$ with an expanded graph shown on the right. Note that the peaks associated with the intergrain ordering are barely discernible over the noise.

sum over all nearest-neighbor grains and $\sum_{\langle ij \rangle \in I \Gamma J}$ denotes the sum over all nearest-neighbor spins connecting grains I and J .

Within the RGA, we can specify the state of the system in terms of the L^2 variables $\sigma_I = \pm 1$ that denote the orientation of the spins in the I th grain. We can then write the Hamiltonian of the system as

$$\mathcal{H}_{\text{RGA}} = E_0 - J_{\text{eff}} \sum_{\langle I I' \rangle} \sigma_I \sigma_{I'} - H_{\text{eff}} \sum_I \sigma_I, \quad (11)$$

where we have defined

$$J_{\text{eff}} = J A_g = J L' z, \quad (12)$$

$$H_{\text{eff}} = H N_g = H L'^2 z, \quad (13)$$

$$E_0 = -J' [3zL'^2 - L'(L' + 2z)], \quad (14)$$

where E_0 is the exchange energy due to the intragrain coupling, which in the RGA is simply a constant. In the RGA our model therefore reduces to the 2D Ising model and value of T_c is simply given by

TABLE I. Intragrain order temperature T'_c at which the peak in the heat capacity occurs as a function of the grain dimensions L' and z . The values in parentheses are calculated from the scaling relations Eqs. (7) and (9).

L'	5	8	10	$L' = \infty (J' = 1)$
$z=1$	1.78 (2.04)	(2.12)	2.04 (2.15)	(2.269)
$z=5$	3.15 (3.35)	(3.57)	3.65 (3.66)	4.03 ± 0.01 (4.028)
$z=8$	(3.50)	3.7 (3.75)	(3.84)	4.25 ± 0.05 (4.246)
$z=10$	3.4 (3.55)	(3.80)	3.9 (3.90)	4.32 ± 0.01 (4.317)

$$T_c = 2.269 J_{\text{eff}} = 2.269 J L' z. \quad (15)$$

The numerical estimates of T_c are plotted for $z=5$ and 10 as a function of $J_{\text{eff}} = J A_g = J L' z$ in Fig. 11. This shows that for $z \geq 5$ and $J \times L' \times z \leq 1$, $T_c \approx 2.269 J_{\text{eff}}$ indicating that the results are in good agreement with the predictions of the RGA. We note also that the slope of lines used to fit the data shown in Fig. 7 for $z=1$ are very close to $2.269 L'$, the value predicted by the RGA.

If we use $T'_c(z, L) \geq T_c(z, L)$ as our criteria for the validity of the RGA up to the Curie temperature, $T_c(z, L)$, then we obtain the following result:

$$\frac{2.0f(z)}{1 + 1.13f(z)/L'} \approx 2.0f(z) \geq \frac{J_{\text{eff}}}{J'} = \frac{J L' z}{J'}. \quad (16)$$

Approximating $f(5)=0.892$ and $f(10)=0.957$ as unity and setting $J'=1$, the above approximation reduces to $J_{\text{eff}} \ll 2.0$.

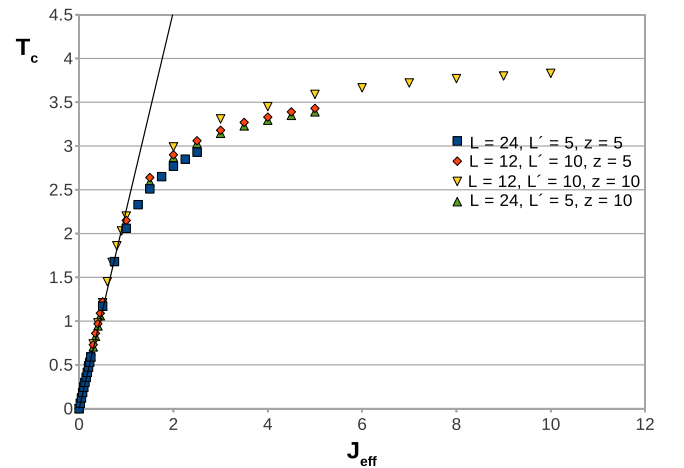


FIG. 11. (Color online) T_c vs $J \times L' \times z$ in the multilayer case for different J , L' , and z (values shown in the legend). Straight line has a slope of $2.269 = T_c / J_{\text{eff}}$ equivalent to the result expected for the 2D Ising model.

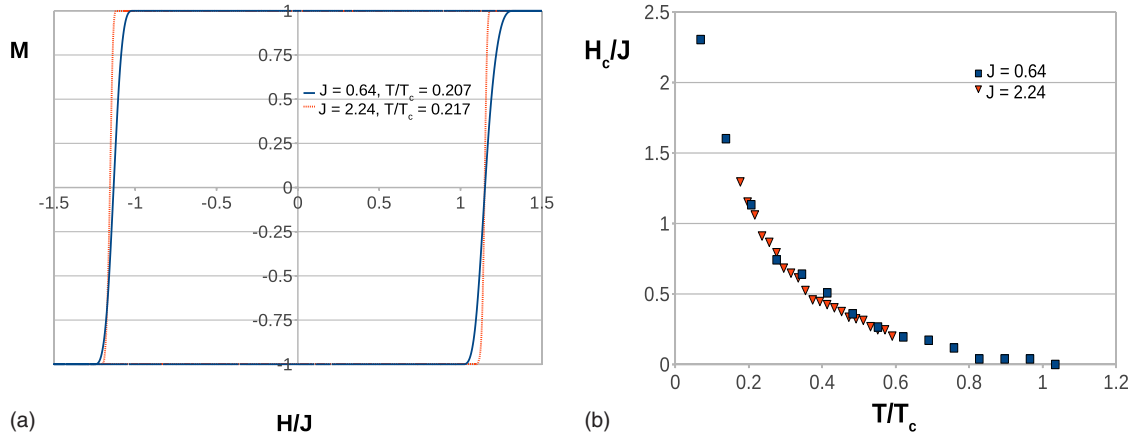


FIG. 12. (Color online) (a) M - H loops for the 2D Ising model using the standard Metropolis algorithm with the magnetization plotted as a function of H/J for two similar values of T/T_c and (b) two plots of the scaled coercive field H_c/J plotted as a function of the reduced temperature T/T_c for two values of J as shown in the legend.

This is consistent with the results plotted in Fig. 11, which shows the values of T_c deviating from the result predicted by the RGA at $J_{\text{eff}} \approx 1.0$. Using $f(1)=0.5$ the above inequality reduces to $J \ll 1.0/L'$ for $z=1$, which is again consistent with the data presented in Fig. 7, and shows the values of T_c deviating from the result predicted by the RGA at $J \approx 0.1$ and 0.05 for $L'=5$ and 10 , respectively. These results suggest that the RGA breaks down for some temperature $T < T'_c$ for $J_{\text{eff}}/J' \gtrsim f(z)$ and therefore must be applied with some caution in describing the properties of granular films in this regime.

IV. M - H LOOPS

Hysteresis is an inherently nonequilibrium phenomenon, a fact that is reflected in the observed dependence of the coercive field on the measurement sweep rate. In the case of the Heisenberg model, there are a number of simulation results that indicate a reliable estimate of the coercivity can be obtained using a simple Metropolis algorithm.^{13,17} In addition, it is possible to link the Metropolis algorithm to Langevin micromagnetics through the Fokker-Planck equation and quantify the time associated with each Monte Carlo step.^{18,19} For the Ising model the situation is somewhat more complicated with the coercive field being strongly dependent on the particular algorithm used (e.g., Metropolis, Wolff, etc.) as well as the number of Monte Carlo steps.²⁰ The results in this section are therefore exploratory from which only tentative conclusions can be made regarding trends rather than absolute values. Comparative calculations on the Heisenberg model with anisotropy will be reported elsewhere.

Two sample M - H loops together with a plot of the coercivity versus temperature calculated from the Metropolis algorithm are presented in Fig. 12 for the 2D Ising model for two values of exchange constant J . The coercivity data are plotted in terms of the reduced parameters H_c/J and T/T_c and show the data collapse expected on the basis of simple scaling arguments with $\lim_{T \rightarrow T_c} H_c \approx 0$. A similarly shaped curve is found from micromagnetic simulations of anisotropic Heisenberg model systems²¹ which correctly accounts for the dynamics associated with hysteresis.

In the case of the granular Ising model, the low acceptance rates for the individual spin flips for $T \ll T'_c$, means that calculating the coercive field using the Metropolis algorithm is computationally far more demanding than in the case of 2D Ising model, while the Wolff algorithm, while ideal for efficiently sampling states close to equilibrium, yields a value of the coercive field that is effectively zero down to the lowest temperatures.

In order to construct a MC scheme that allows for the coherent reversal of individual grains in a manner that respects ergodicity and detailed balance, we consider a variant of the Wolff cluster algorithm used in the previous section. Writing the energy for a given spin configuration in an applied magnetic field H as $\mathcal{H} = \mathcal{H}_0 + \mathcal{H}'$, where we define

$$\mathcal{H}_0 = -J' \sum_I \sum_{\langle ij \rangle \in I} S_i S_j, \quad (17)$$

$$\mathcal{H}' = -J \sum_{\langle IJ \rangle} \left(\sum_{\langle ij \rangle \in I \cap J} S_i S_j \right) - H \sum_i S_i. \quad (18)$$

The clusters are constructed using only the intragrain portion of the exchange energy, \mathcal{H}_0 , with the acceptance ratio determined by the Boltzmann factor $e^{-\beta \Delta \mathcal{H}'}$. While it can be readily shown this algorithm respects both ergodicity and detailed balance, constructing the clusters based on \mathcal{H}_0 ensures that the maximum cluster size cannot exceed the size of a single grain. The motivation for this modified Wolff algorithm is based on the assumption that the spins within a single grain equilibrate much more rapidly than the individual grains and is constructed such that the individual grains maintain a “quasiequilibrium” as the grains order collectively in response to the changes in the applied magnetic field.

M - H loops were calculated using this modified algorithm with $J'=1.0$ for several values of J with lattice dimensions $L=L'=10$ and $z=1$. The resulting coercive fields vs temperature are shown in Fig. 13 in terms of the reduced parameters $H_{\text{eff}}^c/J_{\text{eff}}$ and T/T_c , where J_{eff} and H_{eff}^c are defined by Eqs. (12) and (13) and T_c is defined by the peak position in the

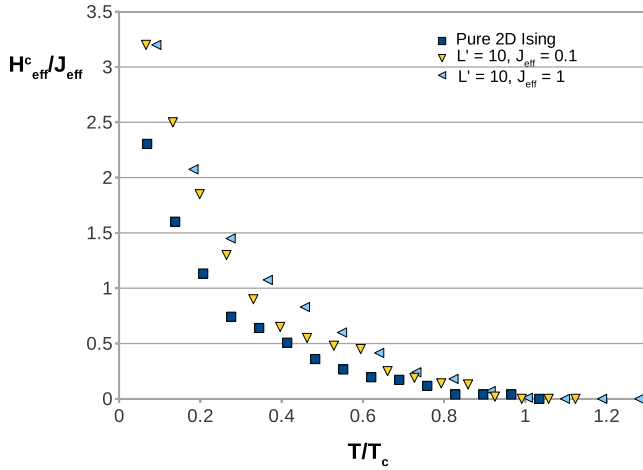


FIG. 13. (Color online) Plots of the scaled coercive field $H_{\text{eff}}^c/J_{\text{eff}}$ [see Eqs. (12) and (13)] plotted as a function of the reduced temperature T/T_c for several values of J (shown in the legend) with $z=1$ and $L'=10$.

susceptibility data. Data for the 2D Ising model are also included for comparison. The results show some degree of the data collapse expected if the RGA were valid; however, the coercivity for the granular Ising model is seen to deviate systematically from the predictions of the RGA as J_{eff} is increased. While it is tempting to attribute this deviation to the increasing significance of the internal grain degrees of freedom as the intergrain coupling increases, in a manner analogous to the results of the previous section, the possibility that the deviation is simply due to the inherent inadequacies of the Ising model in determining the coercive field cannot be ruled out. More detailed studies of the effect of the internal grain degrees of freedom on the coercivity within the context of the anisotropic Heisenberg model are currently in progress.

V. CONCLUSIONS

We have presented the results from a series of Monte Carlo simulations of an exchange coupled Ising model of a highly anisotropic, granular media. The principal focus of these studies is to examine the interplay between the fluctuations within the grains, where the spins are strongly coupled and the fluctuations associated with the more weakly coupled grains. Various thermodynamic quantities that exhibit signatures associated with the onset of the ordering of the spins within a grain and with the onset of ordering between the individual grains were calculated. From these quantities, estimates of the temperatures at which the intragrain and intergrain order occur, denoted as T'_c and T_c , respectively, were obtained. The simulations were performed using the Wolff cluster algorithm to address the difficulties associated with equilibrating a system with two distinct energy scales.

Two principal results emerged from these studies. First, it was found that the intragrain transition temperature T'_c , esti-

mated from the peak in the heat capacity, could be approximated by the formula

$$\frac{T'_c}{T_0} \approx \frac{2.0f(z)}{1 + 1.13f(z)/L'}, \quad (19)$$

where T_0 denotes the Curie temperature for the bulk material (i.e., $J=J'$ and $z \rightarrow \infty$) and $f(z)$ is defined in Eq. (7). Second, it was found that the intergrain transition temperature T_c , estimated from the peak in the susceptibility, was consistent with the RGA result, $T_c \approx 2.27J_{\text{eff}}$, provided $J_{\text{eff}}/J' \lesssim f(z)$, where $J_{\text{eff}}=JL'z$ denotes the effective coupling between the grains in the RGA approximation. In this regime, the temperatures at which the intergrain and intragrain ordering occur are well separated with $T_c \lesssim T'_c/2$, and the fluctuations within the individual grains do not play a significant role in the intergrain ordering.

We have also simulated $M-H$ loops for the granular Ising model to examine the role of the intragrain fluctuations on the coercive field. The simulations were performed using a modified Wolff algorithm designed to capture phenomena on a time scale associated with grain reversal. The results for the coercive field shown in Fig. 13 show a systematic deviation with increasing intergrain coupling. More detailed simulations based on the Heisenberg model are currently in progress to better model the nonequilibrium behavior of granular recording media.

In conclusion, these simulations provide quantitative estimates of the temperatures at which we may expect to observe the onset of intergrain and intragrain ordering in highly anisotropic granular magnetic films. The results of these simulations also help delineate the regime for which the RGA, implicit in micromagnetics studies, may be applied with some confidence. Specifically we show that the RGA is valid provided $T \lesssim 0.5T'_c$ and $J_{\text{eff}}/J' \lesssim f(z)$ with T'_c and $f(z)$ given by Eqs. (7) and (9), respectively. Finally, while estimates of the coercivity obtained from these simulations suggest that the RGA is valid provided the *effective* coupling between the grains J_{eff} is small relative to the intragrain coupling J' , these simulations yield at best qualitative estimates of the coercive fields. It is hoped that these results can serve as a useful guide toward understanding the level of detail required to accurately model magnetic recording processes that involve a significant interplay between thermal fluctuations and intergrain media exchange coupling as found in promising new technologies such as HAMR as well as, for example, exchange coupled composite media.²²

ACKNOWLEDGMENTS

We thank Johannes van Ek for enlightening discussions on recording media and the HAMR concept. This work was supported by the Natural Science and Engineering Research Council of Canada (NSERC), the Canada Foundation for Innovation (CFI), and the Atlantic Computational Excellence Network (ACEnet).

- ¹W. F. Brown, *Phys. Rev.* **130**, 1677 (1963).
- ²M. Plumer, J. van Ek, and D. Weller, *The Physics of Ultra-High-Density Magnetic Recording* (Springer-Verlag, Berlin, 2001).
- ³R. E. Rottmayer, S. Batra, D. Buechel, W. A. Challener, J. Hohlfield, Y. Kubota, L. Li, B. Lu, C. Mihalcea, K. Mountfield, K. Pelhos, C. Peng, T. Rausch, M. A. Seigler, D. Weller, and X. Yang, *IEEE Trans. Magn.* **42**, 2417 (2006).
- ⁴A. F. Torabi, J. van Ek, E. Champion, and J. Wang, *IEEE Trans. Magn.* **45**, 3848 (2009).
- ⁵G. Grinstein and R. H. Koch, *Phys. Rev. Lett.* **90**, 207201 (2003).
- ⁶O. N. Mryasov, U. Nowak, K. Y. Guslienko, and R. W. Chantrell, *Europhys. Lett.* **69**, 805 (2005).
- ⁷N. Kazantseva, D. Hinzke, U. Nowak, R. W. Chantrell, U. Atxitia, and O. Chubykalo-Fesenko, *Phys. Rev. B* **77**, 184428 (2008).
- ⁸S. Rohart, P. Campiglio, V. Repain, Y. Nahas, C. Chacon, Y. Girard, J. Lagoute, A. Thiaville, and S. Rousset, *Phys. Rev. Lett.* **104**, 137202 (2010).
- ⁹R. H. Kodama and A. E. Berkowitz, *Phys. Rev. B* **59**, 6321 (1999).
- ¹⁰X. Z. Cheng, M. B. A. Jalil, and H. K. Lee, *IEEE Trans. Magn.* **43**, 2899 (2007).
- ¹¹H. Kachkachi, *J. Magn. Magn. Mater.* **316**, 248 (2007).
- ¹²J.-G. Zhu, H. Yuan, S. Park, T. Nuhfer, and D. E. Laughlin, *IEEE Trans. Magn.* **45**, 911 (2009).
- ¹³J. Mazo-Zuluaga, J. Restrepo, F. Muñoz, and J. Mejía-López, *J. Appl. Phys.* **105**, 123907 (2009).
- ¹⁴D. A. Garanin and H. Kachkachi, *Phys. Rev. B* **80**, 014420 (2009).
- ¹⁵M. E. J. Newman and G. T. Barkema, *Monte Carlo Methods in Statistical Physics* (Oxford University Press, Oxford, 1999).
- ¹⁶X. T. Pham Phu, V. T. Ngo, and H. T. Diep, *Surf. Sci.* **603**, 109 (2009).
- ¹⁷J. P. Pereira Nunes, M. Bahiana, and C. S. M. Bastos, *Phys. Rev. E* **69**, 056703 (2004).
- ¹⁸U. Nowak, R. W. Chantrell, and E. C. Kennedy, *Phys. Rev. Lett.* **84**, 163 (2000).
- ¹⁹X. Z. Cheng, M. B. A. Jalil, H. K. Lee, and Y. Okabe, *Phys. Rev. Lett.* **96**, 067208 (2006).
- ²⁰M. G. Mazza, K. Stokely, E. G. Strelakova, H. E. Stanley, and G. Franzese, *Comput. Phys. Commun.* **180**, 497 (2009).
- ²¹M. L. Plumer, J. van Lierop, B. W. Southern, and J. P. Whitehead, *J. Phys.: Condens. Matter* **22**, 296007 (2010).
- ²²R. H. Victora and X. Shen, *IEEE Trans. Magn.* **41**, 2828 (2005).